Bioconjugate Chemistry

pubs.acs.org/bc
Article

Mannosamine-Modified Poly(lactic-*co*-glycolic acid)-Polyethylene Glycol Nanoparticles for the Targeted Delivery of Rifapentine and Isoniazid in Tuberculosis Therapy

Cong Peng,[†] Haopeng Luan,[†] Qisong Shang, Wei Xiang, Parhat Yasin, and Xinghua Song*

Cite This: *Bioconjugate Chem.* 2025, 36, 1021−1033
Read Online

ACCESS | Metrics & More | Article Recommendations

ABSTRACT: Tuberculosis, caused by *Mycobacterium tuberculosis*, is the leading cause of mortality attributed to a single infectious agent. Following macrophage invasion, M. tuberculosis uses various mechanisms to evade immune responses and to resist antituberculosis drugs. This study aimed to develop a targeted drug delivery system utilizing mannosamine (MAN)-modified nanoparticles (NPs) composed of poly(lactic-*co*-glycolic acid)−polyethylene glycol (PLGA−PEG), loaded with rifapentine and isoniazid, to enhance macrophage-directed therapy and enhance bacterial elimination. PLGA−PEG copolymer was modified with mannosamine through an amidation reaction. Rifapentine- and isoniazid-loaded PLGA−PEG-MAN NPs were synthesized by using the double emulsion solvent evaporation technique. The NPs exhibited an average particle size of 117.67 nm and displayed favorable physicochemical properties without evidence of cellular or hemolytic toxicity. The drug loading rates were 11.73% for rifapentine and 5.85% for isoniazid. Sustained drug release was achieved over a period exceeding 72 h, with antibacterial activity remaining intact during encapsulation. Synergistic bactericidal effects were noted. Additionally, mannosamine-modified NPs enhanced the phagocytic activity of macrophages via mannose receptor-mediated endocytosis, thereby improving drug delivery efficiency and significantly boosting the antibacterial efficacy of the NPs within macrophages. Pathological staining and biochemical analysis of rat organs following intravenous injection indicated that the NPs did not cause any significant toxic side effects in vivo. The findings of this study indicate that mannosamine-modified PLGA−PEG NPs loaded with rifapentine and isoniazid represent a promising drug delivery system for targeting macrophages to enhance the efficacy of antitubercular therapy.

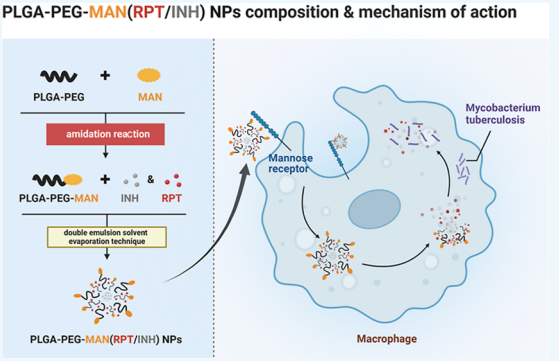

1. INTRODUCTION

Tuberculosis (TB), a chronic infectious disease caused by *Mycobacterium tuberculosis* (MTB), is projected to re-emerge as the leading global cause of mortality from a single infectious agent by 2023, three years after the emergence of the COVID-19 pandemic.[1] It is anticipated to cause nearly twice the number of fatalities as AIDS.[2]

MTB is a facultative intracellular pathogen that primarily resides within macrophages. It uses multiple strategies to evade immune-mediated and macrophage-derived killing mechanisms, including inhibition of phagosome-lysosome fusion, resistance to oxidative and nitrosative stress, suppression of host immune responses, and modulation of autophagy and metabolic pathways following macrophage invasion.[3−6] Infection of macrophages by MTB often leads to the formation of granulomas, which serve to localize and contain the infection by restricting pathogen dissemination.[7] However, this localized microenvironment impairs blood circulation, hindering drug penetration, limiting drug penetration, and reducing therapeutic delivery to infected macrophages.[8] Additionally, MTB employs efflux pumps to actively expel antibiotics, further complicating treatment.[9] These challenges necessitate the use of higher drug doses to achieve effective bactericidal concentrations within macrophages. However, the limited bioavailability of conventional oral and injectable formulations requires even higher doses, increasing the risk of dose-dependent toxicities and adverse side effects.

Macrophages are equipped with numerous phagocytic receptors, including the mannose receptor, fucosyl receptor, scavenger receptor, Fc receptors, folate receptor, hyaluronic acid receptor, tuftsin receptor, formyl peptide receptor, and various lectin-like receptors.[10,11] Ligands binding to these receptors facilitate macrophage phagocytosis, providing a

Received: February 11, 2025
Revised: March 26, 2025
Accepted: April 9, 2025
Published: April 22, 2025

https://doi.org/10.1021/acs.bioconjchem.5c00062
Bioconjugate Chem. 2025, 36, 1021−1033

promising approach for the targeted delivery of anti-TB drugs. Among these ligands, mannose is widely used due to its dual benefits. It not only improves phagocytosis through interaction with mannose receptors but also enhances bactericidal activity by promoting cytokine secretion and promoting antigen presentation.[12]

Effective drug delivery to macrophages requires the use of suitable drug delivery carriers. Polymer nanoparticles (NPs) have emerged as ideal carriers for drug delivery systems due to their favorable storage stability, tunable physicochemical properties, high drug-loading capacity, biocompatibility, and ease of surface modification.[13,14] Among these polymers, poly(D,L-lactide-*co*-glycolide) (PLGA) has been approved by the U.S. Food and Drug Administration (FDA) for biomedical applications.[15] Additionally, polyethylene glycol (PEG), a hydrophilic polymer, when combined with hydrophobic PLGA, forms PLGA−PEG copolymers, which exhibit enhanced stability and sustained drug release properties.[16] The drug release rate can be modulated by adjusting the molecular weight and the ratio of PEG to PLGA.[17] Liang et al.[18] prepared rifapentine-loaded PLGA−PEG NPs using solvent evaporation and demonstrated that passive targeting of macrophages based on the NPs' inherent physicochemical properties was relatively inefficient. In this study, we modified PLGA−PEG with mannosamine as a ligand to build upon its passive targeting capability and further enhance its targeting performance through a ligand−receptor-mediated mechanism. Pi et al.[19] developed a mannose-functionalized graphene oxide nanodelivery system, and in vitro studies demonstrated its effective macrophage-targeting capability. However, its drug encapsulation was limited to fat-soluble compounds. In contrast, PLGA−PEG-MAN enables the dual delivery of both fat- and water-soluble drugs through a double emulsion solvent evaporation method. Similar to many drug-loaded NPs, PLGA−PEG-MAN also suffers from a low loading efficiency for water-soluble drugs. For example, the encapsulation efficiency of isoniazid in the hybrid lipopolysaccharide NPs prepared by Sumaila et al.[20] was only 4.55%, while that of levofloxacin in the cyclodextrin—Curdlan conjugated NPs developed by Yunus et al.[21] was merely 4%. Notably, Puri et al.[22] enhanced the drug loading (DL) of INH by dissolving it in a PVA aqueous solution as the inner aqueous phase during the preparation of NPs via the double emulsion solvent evaporation method, offering valuable inspiration for our formulation approach.

In this study, mannosamine (MAN) was conjugated to the terminal carboxyl group of PLGA−PEG to synthesize a PLGA−PEG-MAN polymer. Using the double emulsion solvent evaporation method, the polymer was used to encapsulate the hydrophilic antituberculosis drug isoniazid (INH) in the inner aqueous phase of the NPs, while the hydrophobic antituberculosis drug rifapentine (RPT) was encapsulated in the oil phase. This process resulted in dual drug-loaded polymer NPs with macrophage-targeting capabilities. The inclusion of MAN facilitated targeted delivery by enhancing macrophage uptake, thereby increasing the intracellular concentration of both antituberculosis drugs. Additionally, the polymer NPs provided sustained intracellular drug release, contributing to the eradication within macrophages while reducing the risk of dose-dependent toxicity and adverse effects.

2. MATERIALS AND METHODS

2.1. Materials Preparation. PLGA−PEG-COOH (lactide/glycolide ratio of 50:50, PLGA: M_W 19000, PEG: M_W 2000) was purchased from Pengsheng Biotechnology Co., Ltd. (Shanghai, China). RPT (97% purity) and INH (99% purity) were obtained from Solarbio Science & Technology Co., Ltd. (Beijing, China). Dulbecco's Modified Eagle's Medium (DMEM), trypsin−EDTA, fetal bovine serum, and penicillin−streptomycin solution were supplied by Thermo Fisher Scientific (Waltham, MA, USA). Unless otherwise stated, all other chemicals and reagents were procured from Sigma Chemical (St. Louis, MO, USA).

2.2. Preparation of the PLGA−PEG-MAN Polymer. The PLGA−PEG-MAN polymer was synthesized by activating the terminal carboxyl group of PLGA−PEG through the carbodiimide-mediated amidation method to facilitate bonding with the amino group of MAN. A total of 50 mg of PLGA−PEG was dissolved in 20 mL of dimethyl sulfoxide, followed by the addition of 50 mg of 1-(3-(dimethylamino)propyl)-3-ethylcarbodiimide (EDC) and 60 mg of *N*-hydroxysuccinimide (NHS). The mixture was stirred at 37 °C for 6 h to activate the carboxyl group. Subsequently, 10 mg of MAN was added to the mixture, which was stirred for 24 h under a nitrogen atmosphere. The resulting solution was dialyzed against pure water for 72 h and then centrifuged and freeze-dried for subsequent use. Structural verification of the synthesized polymer was performed using Fourier Transform Infrared spectroscopy (Thermo Fisher, USA), proton nuclear magnetic resonance (^{1}H NMR, Bruker, Switzerland), and X-ray photoelectron spectroscopy (XPS, Thermo Fisher, USA).

2.3. Preparation of Dual Drug-Loaded Macrophage-Targeted NPs. The dual-drug-loaded NPs were fabricated using the double emulsion solvent evaporation method.[23] For the inner aqueous phase, 10 mg of INH was dissolved in 200 μL of 3% (w/v) poly(vinyl alcohol) (PVA) aqueous solution and vortexed until completely dissolved. For the oil phase, 80 mg of PLGA−PEG-MAN and 10 mg of RPT were dissolved in 2 mL of dichloromethane. The two phases were mixed, and ultrasonic emulsification (S-450D Digital Sonifier, Branson, USA) was performed in an ice bath (ultrasonic time: 2 s; interval: 3 s; power: 90 W; repeated for 80 cycles) to form a water-in-oil (W/O) primary emulsion.

The resulting emulsion was then added to 15 mL of a 2% (w/v) PVA aqueous solution, followed by ultrasonic emulsification under the same conditions to produce a water-in-oil-in-water (W/O/W) double emulsion. The mixture was stirred mechanically at 400 rpm for 4 h and washed by using a 10 kDa ultrafiltration tube. The resulting pellet was collected and freeze-dried, yielding RPT- and INH-loaded nanospheres designated as PLGA−PEG-MAN (RPT/INH) NPs.

Using variations in the composition of the internal aqueous and oil phases, additional NPs were prepared, including non-MAN-modified nondrug-loaded nanospheres (PLGA−PEG NPs), MAN-modified nondrug-loaded nanospheres (PLGA−PEG-MAN NPs), non-MAN-modified dual-drug-loaded nanospheres (PLGA−PEG (RPT/INH) NPs), MAN-modified INH-loaded nanospheres (PLGA−PEG-MAN (INH) NPs), and MAN-modified RPT-loaded nanospheres (PLGA−PEG-MAN (RPT) NPs).

2.4. Particle Size, Polydispersity Index, and Zeta Potential. Particle size (PS) and polydispersity index (PDI) of the NPs were evaluated by using dynamic light scattering with

https://doi.org/10.1021/acs.bioconjchem.5c00062
Bioconjugate Chem. 2025, 36, 1021−1033

a PS analyzer (Malvern Panalytical, UK). The Zeta potential (ZP) was determined based on the principle of electrophoretic light scattering. Prior to analysis, the NPs were diluted to an appropriate concentration by using deionized water. Each sample was analyzed in triplicate.

2.5. Transmission Electron Microscopy. The morphology of NPs was characterized by using transmission electron microscopy (Tecnai G2 F20, FEI, USA). For analysis, the prepared NPs were suspended in deionized water and deposited onto copper mesh support grids by using a microdropper. The samples were dried at a low temperature, stained with 2% (w/v) phosphotungstic acid, and dried again before being imaged under the microscope.

2.6. High-Performance Liquid Chromatography Assay. The concentrations of RPT and INH were quantified using an HPLC system comprising a chromatograph (Arc HPLC, Waters, USA), a UV detector (2998, Waters, USA), and a SinoPak C18 column (4.6 × 150 mm, 5 μm, Elite, China). Chromatographic separation was conducted under the following conditions: 15 min of gradient elution at a flow rate of 1.0 mL/min, a column temperature of 30 °C, and a detection wavelength of 255 nm. The injection volume was 10 μL, and the mobile phase consisted of solvent A (methanol) and solvent B (0.1% formic acid in water).

2.7. Drug Entrapment Efficiency and Drug Loading. Entrapment efficiency (EE) and DL were quantified using an HPLC analysis. The procedure was as follows: 1 mg of NPs was accurately weighed, followed by the addition of 1 mL of dichloromethane. The mixture was vortexed for 10 s at 1000 rpm and sonicated at 500 W for 10 min. Dichloromethane was then completely removed by blowing nitrogen at room temperature. Subsequently, 2 mL of chromatographic methanol was added to the test tube, and the mixture was vortexed for 10 s at 1000 rpm, followed by sonication at 500 W for an additional 10 min.

The resulting solution was filtered through a 0.22 μm membrane filter and transferred to an HPLC sample vial. Each NP formulation was analyzed in triplicate. The concentrations of RPT and INH were determined by detecting the peak area using HPLC, using a preestablished standard curve equation under specified chromatographic conditions. EE and DL values were computed using the following formulas: %EE = (drug content in NPs)/(drug added), %DL = (drug content in NPs)/(NP weight).

To evaluate the stability of NPs, samples were kept in a sealed stable chamber at a temperature of 25 °C for a duration of 90 days. Periodically, samples were gathered to determine PDI, EE, and PS.

2.8. In Vitro Drug Release. The drug release profile of NPs was evaluated using the dialysis bag method. NPs or an equivalent mass of the free drug (corresponding to the amount encapsulated within the NPs) was mixed with 3 mL of phosphate-buffered saline (PBS). The mixture was placed into a dialysis bag with a molecular weight cutoff of 8000−14,000 Da. The dialysis bag was then immersed in a centrifuge tube containing 20 mL of dialysis fluid (0.2% v/v Tween 80 in PBS, pH 7.4). The tube was incubated at 37 °C in the dark with continuous shaking at 100 rpm.

At predetermined time intervals, 1 mL of the dialysate was withdrawn from the centrifuge tube and replaced with an equal volume of fresh dialysis fluid. The concentration of the released drug in the dialysate was determined using HPLC under the previously described chromatographic conditions. Each sample group was tested using three independent release setups, and the average values were used to construct the drug release curve.

2.9. Anti-TB Studies. The antitubercular activity of NPs against MTB was assessed using a 96-well plate resazurin staining method, modified from a previously reported protocol.[24] In this assay, 200 μL of sterile PBS was added to the peripheral wells of a 96-well plate. The NPs or free drug were suspended in 7H9 broth and added to column 3. Serial dilutions were conducted from column 3 to column 10, and 100 μL of an MTB bacterial suspension was added to each well.

Negative controls were prepared by adding 200 μL of sterile broth to each well in column 2, while positive controls consisted of 100 μL of MTB bacterial suspension combined with 100 μL of sterile broth in each well of column 11. Six replicate rows were established for each set of samples. The plates were incubated at 37 °C for 7 days. After incubation, 20 μL of the 0.02% (w/v) resazurin indicator was added to each well, and the plates were incubated overnight to observe color changes indicative of metabolic activity. The minimum inhibitory concentration (MIC) was defined as the lowest concentration of the NPs or free drug that prevented a color change in the resazurin indicator from blue to pink.

2.10. Cell Culture Studies. *2.10.1. Cytotoxicity Test.* The cytotoxicity of NPs and free drugs was evaluated by using the CCK-8 assay. RAW 264.7 cells were incubated with NPs or free drugs (equivalent to the drug amount contained in PLGA−PEG-MAN (RPT/INH) NPs) at 37 °C for 24 h at final NP concentrations of 50, 100, 200, and 400 μg/mL. The concentrations of NPs were selected based on previously reported findings.[25] Following incubation, 10 μL of a CCK-8 solution was added to each well, and the incubation was continued for an additional hour. The absorbance at 450 nm was measured by using a microplate reader.

2.10.2. Hemolytic Study. The biocompatibility of NPs with erythrocytes was assessed by using a hemolytic toxicity assay. Rats were intraperitoneally anesthetized with 3 mg/100 g of pentobarbital sodium, followed by blood sampling from the abdominal aorta, which was completed, and sacrificed by carbon dioxide asphyxiation. Red blood cells were isolated from fresh blood by centrifugation and resuspended in normal saline. The NPs were resuspended in saline to prepare nanosuspensions at various concentrations (0.5−3.0 mg/mL), which were then mixed with the erythrocyte suspension to allow interaction. Triplicate samples were prepared for each concentration of the NP formulation.

After coincubation for 30 min, the mixtures were centrifuged, and the supernatants were transferred to quartz cuvettes for absorbance measurement at λ = 541 nm. The hemolysis ratio was calculated by using the following formula: hemolytic rate (%) = (absorbance of sample − absorbance of saline)/(absorbance of water − absorbance of saline) × 100%.

2.10.3. Cell Uptake Studies. The phagocytosis of NPs by macrophages was assessed using confocal laser scanning microscopy (CLSM) and flow cytometry with RAW 264.7 cells at a concentration of 3×10^5 cells/mL. Fluorescently labeled NPs were prepared by incorporating coumarin 6 (C6) into the oil phase, producing PLGA−PEG@C6 NPs and PLGA−PEG-MAN@C6 NPs. RAW 264.7 cells were seeded in 12-well plates and cultured for 24 h before being cocultured with these fluorescently labeled NPs. The cells were collected

https://doi.org/10.1021/acs.bioconjchem.5c00062
Bioconjugate Chem. 2025, 36, 1021−1033

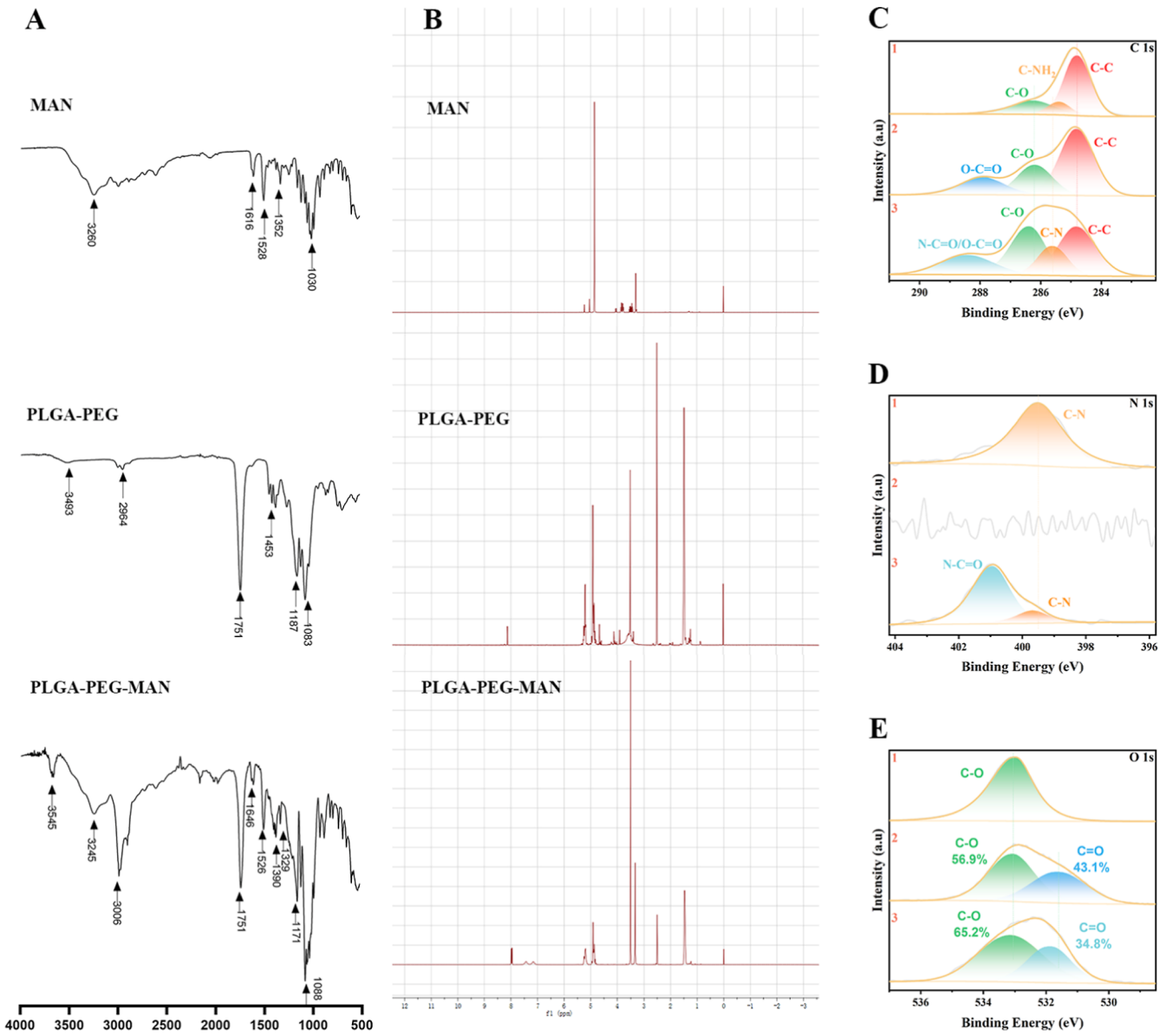

Figure 1. Infrared spectra (A), ^{1}H NMR spectrum (B), and XPS spectra (C−E) of MAN, PLGA−PEG, and PLGA−PEG-MAN.

at 1, 3, 6, 12, and 24 h intervals, washed with PBS, centrifuged, and resuspended for further analysis.

To investigate the role of mannose receptors in the uptake of PLGA−PEG-MAN@C6 NPs, a parallel experiment was conducted in which macrophages were preincubated with 0.05 M mannose for 1 h before exposure to the NPs. All experimental setups included three replicates. Fluorescence intensity was measured by using a flow cytometer (BD Biosciences).

For CLSM analysis, RAW 264.7 cells were seeded on confocal laser scanning dishes at a density of 5×10^4 cells per dish. The cells were incubated with fluorescent NPs for 6 h, washed three times with PBS, fixed with 4% paraformaldehyde, and stained with 5 μg/mL DAPI for 15 min. Cells without fluorescent NPs served as negative controls. Images were captured using a confocal laser scanning microscope (Leica, Germany), with coumarin 6 fluorescence appearing as green and DAPI staining marking the nuclei in blue.

2.10.4. Drug Accumulation in Cultured RAW 264.7 Cells. The intracellular accumulation of drugs following NP uptake was evaluated using RAW 264.7 cells. A cell suspension at a concentration of 1×10^6 cells/mL was seeded in 12-well culture plates and incubated for 12 h. The culture medium was then replaced with a complete medium containing 100 μg/mL PLGA−PEG (RPT/INH) or PLGA−PEG-MAN (RPT/INH) NPs. For comparison, the control group received a complete medium containing the equivalent dose of the free drug present in the PLGA−PEG-MAN (RPT/INH) NPs. Each group was tested in triplicate.

After 1 h of incubation, cells and culture media were collected from the wells. The cells were washed with PBS and centrifuged three times to remove NPs and free drugs from their surfaces. The collected media and wash solutions were analyzed for extracellular drug content using HPLC. The washed cells were resuspended in deionized water and subjected to ultrasonic lysis in an ice bath.[26] The lysates were centrifuged to remove any cellular debris that could interfere with drug quantification. The resulting supernatants were analyzed for intracellular drug content using HPLC.

https://doi.org/10.1021/acs.bioconjchem.5c00062
Bioconjugate Chem. 2025, 36, 1021−1033

Table 1. Physicochemical Characterization of NPs[a]

sample	PS (nm)	PDI	ZP (mV)	EE (%)		DL (%)	
				RIF	INH	RIF	INH
PLGA−PEG NPs	107.07 ± 0.49	0.19 ± 0.03	−19.97 ± 0.43				
PLGA−PEG-MAN NPs	109.23 ± 0.71	0.15 ± 0.04	−16.04 ± 1.84				
PLGA−PEG-MAN(RPT) NPs	111.77 ± 0.61	0.19 ± 0.04	−16.05 ± 0.45	81.83 ± 3.26		11.74 ± 0.22	
PLGA−PEG-MAN(INH) NPs	112.93 ± 0.33	0.16 ± 0.02	−15.80 ± 0.26		41.76 ± 6.40		6.13 ± 0.73
PLGA−PEG (RPT/INH) NPs	113.6 ± 0.22	0.16 ± 0.02	−20.00 ± 0.41	80.37 ± 3.35	40.30 ± 2.42	11.39 ± 0.31	5.71 ± 0.14
PLGA−PEG-MAN(RPT/INH) NPs	117.67 ± 0.98	0.19 ± 0.01	−15.89 ± 0.21	81.80 ± 2.36	40.87 ± 3.56	11.73 ± 0.30	5.85 ± 0.24

[a]Abbreviations: PLGA, poly D, l-lactide-*co*-glycolide; PEG, polyethylene glycol; MAN, mannosamine; NPs, nanoparticles; PS: particle size; PDI, polydispersity index; ZP, zeta potential; EE, encapsulation efficiency; DL, drug loading; RPT, rifapentine; and INH, isoniazid.

2.10.5. Intracellular Inhibition of M. tuberculosis by NPs. RAW 264.7 macrophages were seeded at a density of 1×10^6 cells/mL in 12-well plates and infected with the H37Rv strain at a multiplicity of infection of 1 for 4 h after cell attachment. Following infection, cells were washed with PBS, and fresh medium containing gentamicin was added to eliminate extracellular bacteria. For imaging purposes, RAW 264.7 cells were also cultured in confocal laser scanning dishes and infected with a green fluorescent protein (GFP)-tagged H37Rv strain, following the same protocol. After infection, cells were fixed with 4% paraformaldehyde and stained with DAPI. CLSM was used to capture images, with green fluorescence indicating GFP-labeled bacteria and blue fluorescence marking the nuclei of RAW 264.7 cells. This allowed confirmation of the successful establishment of the intracellular H37Rv infection model in RAW 264.7 macrophages.

PLGA−PEG (RPT/INH) and PLGA−PEG-MAN (RPT/INH) NPs were resuspended in complete medium to a final concentration of 2 μg/mL. Free INH and RPT were diluted to match the drug concentrations present in the PLGA−PEG-MAN (RPT/INH) NP group. Both the NP suspensions and free drug solutions were added to RAW 264.7 cells infected with intracellular H37Rv and incubated for 72 h. After incubation, the cells were washed three times with PBS and lysed with 0.03% SDS for 10 min. The resulting lysates were serially diluted and plated on Middlebrook 7H11 agar. Bacterial colonies were counted after incubation for 21 days at 37 °C. A RAW 264.7 intracellular H37Rv-infected group without treatment was included as a control.

2.11. In Vivo Biosafety Study. Sprague−Dawley rats (body weight 265 ± 24 g) were obtained from the Animal Center of Xinjiang Medical University. Animal anesthesia, handling, and welfare procedures were consistent with those described in the Hemolysis Study section. The rats were randomly divided into three groups: a PLGA−PEG-MAN (RPT/INH) NPs group, a free RPT and INH group, and a control group. Each rat received a single intravenous injection, with the NPs group administered 10 mg/100 g of NPs. The free drug group received RPT and INH at equivalent doses to those encapsulated in the NPs group. The control group was given the same volume of normal saline. Three days after administration, blood samples were collected from the abdominal aorta under pentobarbital anesthesia. The heart, liver, spleen, lungs, and kidneys were then harvested. These organs were sectioned and stained with hematoxylin and eosin (H&E) for histopathological examination using an optical microscope. Blood biochemical analyses were performed for all groups, focusing on five indicators: alanine aminotransferase (ALT), aspartate aminotransferase (AST), blood urea nitrogen, total bilirubin, and uric acid.

3. RESULTS AND DISCUSSION

3.1. Characterization of Polymers. The infrared spectra of PLGA−PEG, MAN, and PLGA−PEG-MAN are depicted in Figure 1A. In the PLGA−PEG spectrum, the absorption peak at 1751 cm^{-1} corresponds to the carbonyl group (C═O) present in the PLGA ester and carboxyl groups. The peak observed at 3493 cm^{-1} is attributed to the terminal O−H group of the copolymer. Peaks near 2964 cm^{-1} are associated with the C−H bonds of methyl and methylene groups in the PLGA and PEG chain segments, while the absorption in the range of 1083−1187 cm^{-1} corresponds to the C−O−C and C−O bonds of the carboxylic bond, consistent with previous findings.[25] In the MAN spectrum, two distinct peaks were observed: one at 3260 cm^{-1}, representing the O−H groups, and another at 1030 cm^{-1}, corresponding to the C−N groups. The amino group absorption peak was not detected, likely due to the hydrochloride salt form of MAN. The PLGA−PEG-MAN spectrum displays all of the characteristic peaks of PLGA−PEG and MAN, but with noticeable changes and shifts, indicative of the reaction between the two. Notably, the absorption peak at 1646 cm^{-1} in the PLGA−PEG-MAN spectrum represents the carbonyl group (C═O) in the amide bond, confirming that amidation occurred between the carboxyl group of PLGA−PEG and the amino group of MAN, resulting in the formation of the amide bond.

The ^{1}H NMR spectra of PLGA−PEG, MAN, and PLGA−PEG-MAN are depicted in Figure 1B. The peak observed at 8.09 ppm corresponds to the −OH group in carboxylic acid. Peaks at 1.49 and 5.21 ppm represent the methyl and methylene groups of the glycolic acid moiety, respectively. The signal at 4.91 ppm is attributed to the methylene group of the lactic acid fragment, while the peak at 3.62 ppm corresponds to the repeating $-CH_2CH_2O-$ units in PEG. Peaks at 5.24 and 5.05 ppm are associated with the mannose amino-terminal hydrogen signals. Additionally, peaks within the ranges of 3.54−3.41 ppm and 4.04−3.76 ppm are characteristic of methylene protons. These characteristic peaks were all present in the ^{1}H NMR spectrum of PLGA−PEG-MAN, albeit with slight shifts. Furthermore, a new peak at 7.44 ppm in the downfield region was identified as the characteristic signal of amide bond hydrogens, confirming the successful synthesis of PLGA−PEG-MAN.

Figure 1C−E depicts the C 1s, N 1s, and O 1s spectra of MAN, PLGA−PEG, and PLGA−PEG-MAN, respectively. In the C 1s and N 1s spectra of PLGA−PEG-MAN, an N−C═O peak was observed, corresponding to the amide bond. Additionally, in the O 1s spectra, the proportion of C−O bonds in PLGA−PEG-MAN (65.2%) was higher than that in

https://doi.org/10.1021/acs.bioconjchem.5c00062
Bioconjugate Chem. 2025, 36, 1021−1033

Table 2. Stability Evaluation of NPs[a]

sample	time	PS (nm)	PDI	EE (%)	
				RIF	INH
PLGA−PEG-MAN(RPT) NPs	initial	111.77 ± 0.61	0.19 ± 0.04	81.83 ± 3.26	
	1 month	112.35 ± 0.72	0.19 ± 0.06	81.04 ± 3.84	
	3 months	113.17 ± 0.84	0.20 ± 0.05	79.95 ± 4.17	
PLGA−PEG-MAN(INH) NPs	initial	112.93 ± 0.33	0.16 ± 0.02		41.76 ± 6.40
	1 month	113.26 ± 0.69	0.17 ± 0.03		40.96 ± 6.37
	3 months	113.98 ± 0.57	0.16 ± 0.05		39.58 ± 7.02
PLGA−PEG (RPT/INH) NPs	initial	113.6 ± 0.22	0.16 ± 0.02	80.37 ± 3.35	40.30 ± 2.42
	1 month	114.18 ± 0.59	0.16 ± 0.02	79.74 ± 3.56	39.46 ± 5.37
	3 months	111.35 ± 0.82	0.17 ± 0.05	78.58 ± 4.54	37.59 ± 6.40
PLGA−PEG-MAN(RPT/INH) NPs	Initial	117.67 ± 0.98	0.19 ± 0.01	81.80 ± 2.36	40.87 ± 3.56
	1 month	116.59 ± 1.23	0.18 ± 0.03	81.05 ± 3.13	39.26 ± 4.32
	3 months	118.28 ± 1.04	0.19 ± 0.04	80.42 ± 4.65	38.48 ± 5.12

[a]Abbreviations: PLGA, poly d, l-lactide-*co*-glycolide; PEG, polyethylene glycol; MAN, Mannosamine; NPs, Nanoparticles; PS: particle size; PDI, polydispersity index; EE, encapsulation efficiency; RPT, rifapentine; and INH, isoniazid.

PLGA−PEG (56.9%), further corroborating the successful conjugation of MAN with PLGA−PEG.

3.2. NPs Physicochemical Characterization. The physicochemical characteristics of the NPs produced in this study are summarized in Table 1. NPs smaller than 10 nm are typically eliminated through renal filtration and are not reabsorbed.[27] Conversely, NPs larger than 200 nm tend to trigger the complement system, clear quickly from circulation, and accumulate in organs such as the liver and spleen.[28,29] Moghimi et al. proposed that the maximum diameter of spherical NPs should be restricted to 150 nm to prevent splenic filtration.[30] In this study, all the NPs exhibited a PS range between 107 and 117 nm with narrow size distributions (PDI < 0.20), indicating their suitability for therapeutic administration. Chan et al. noted that NPs within this size range are likely to remain in circulation for extended durations, avoid rapid clearance, and are effectively phagocytosed by macrophages, allowing them to remain in tissues for prolonged periods.[31]

The ZP of NPs significantly influences their drug delivery efficiency, particularly their interactions with biological systems and cellular internalization rates. Higher positive or negative ZP values are associated with improved NP stability and uptake compared to neutral or less charged NPs.[32,33] In this study, the ZP values of the prepared NPs ranged from −15 to −20 mV. MAN-modified NPs exhibited lower ZP values compared to their non-MAN-modified counterparts, both for unloaded NPs (−19.97 ± 0.43 mV vs −16.04 ± 1.84 mV) and dual-drug-loaded NPs (−20 ± 0.41 mV vs −15.89 ± 0.21 mV). This difference is attributed to the replacement of the ionizable carboxyl group at the PLGA−PEG terminus with a mannose moiety, forming an amide bond and altering the surface potential.[34] It is generally considered that a ZP in the range of −25 mV to +25 mV indicates good colloidal stability.[35] Positively charged NPs tend to interact more readily with negatively charged serum proteins, leading to higher plasma clearance and potentially triggering capillary embolization.[36,37] In addition, a study on hepatic NP uptake found that PEGylated NPs effectively evaded uptake by liver Kupffer cells due to their low ZP, thereby reducing NP accumulation in the liver.[38] On the other hand, the anionic repulsion on the surface of negatively charged NPs promotes their accumulation in positively charged regions, thereby enhancing their uptake by macrophages.[39] Based on these findings, the NPs we developed not only exhibit stability for prolonged circulation in the bloodstream but also may offer potential advantages in enhancing macrophage uptake.

In all four drug-loaded NPs, the loading rate of the RPT exceeded 11%, while that of the INH was above 5%. A comparison between single-drug and dual-drug NPs revealed no mutual interference in the DL or EE of RPT and INH. Carriers such as polymeric NPs, polymeric micelles, liposomes, and chitosan NPs have been used to deliver drugs including INH, rifampicin, RPT, levofloxacin, and verapamil over the past decade.[40,41] However, most studies have focused on single-drug delivery, with fewer investigations exploring multidrug delivery. Shrivastava et al.[42] reported liposomes coloaded with rifampicin and INH prepared via lipid film hydration. These liposomes had a PS of 1290 nm, a PDI of 0.11, a ZP of −9.1 mV, and encapsulation efficiencies of 84.7% for rifampicin and 31.8% for INH. Compared to these findings, the NPs produced in this study demonstrated superior characteristics, including optimal PS and higher negative ZP, facilitating prolonged circulation and improved macrophage uptake. While the EE for lipid-soluble drugs was comparable, the encapsulation of water-soluble drugs was significantly higher in the present study. Sumaila et al.[20] described lipid-polysaccharide NPs coloaded with rifampicin and INH, modified with mannose residues, and prepared via solvent injection. Although the PS, PDI, and ZP of these NPs were similar to those reported here, their DL rates for rifampicin and INH were only 3.03% and 4.55%, respectively, which are considerably lower than those achieved in the current study, thereby limiting their therapeutic potential.

We monitored PS, PDI, and EE % of NPs for three months. The results showed only minor changes in these parameters, and the statistical analysis showed that these changes were not significantly different ($P > 0.05$) (Table 2). Therefore, it can be concluded that NPs showed good stability over an observation period of at least three months, indicating their potential in practical applications.

3.3. Surface Morphology by TEM. The surface morphology of NPs was analyzed by using TEM, as depicted in Figure 2. All NPs displayed a uniform spherical shape with smooth surfaces and an average diameter of approximately 100 nm. No evidence of particle aggregation was observed, aligning with the PS measurements obtained through DLS. The modification with MAN did not alter the structural integrity

https://doi.org/10.1021/acs.bioconjchem.5c00062
Bioconjugate Chem. 2025, 36, 1021−1033

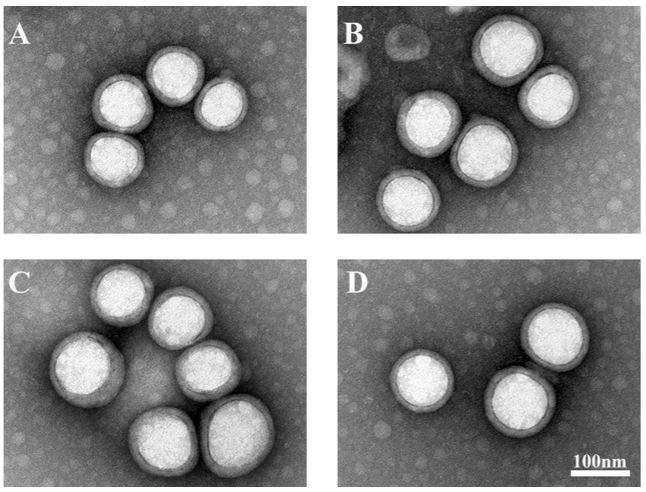

Figure 2. TEM images of NPs (A) PLGA–PEG NPs. (B) PLGA–PEG-MAN NPs. (C) PLGA–PEG (RPT/INH) NPs. (D) PLGA–PEG-MAN (RPT/INH) NPs.

or morphology of the NPs. Similarly, the drug encapsulation process did not affect NP morphology. Spherical NPs have been reported to exhibit the highest cellular uptake by weight, which supports the suitability of the NPs developed in this study for drug delivery applications.[43]

3.4. In Vitro Release Study. The cumulative release profiles of RPT and INH from NPs and free drugs are presented in Figure 3. The free drug release profile exhibited a rapid burst release, with 84% of the RPT released within 3 h and over 95% by 6 h. INH demonstrated a similar rapid release with 95% released within the first hour. In contrast, drug release from NPs was characterized by an initial burst release, followed by a slower, sustained release phase. The drug release data from the NPs were fitted to zero-order, first-order, Higuchi, and Weibull models. The results indicated that the release profiles of both drugs best fit the Weibull model, with correlation coefficients exceeding 0.96. All shape parameters were less than 1, suggesting an initial burst release, followed by a sustained release phase. Notably, the scale parameter for INH release in the dual-drug NPs was smaller than that in the single-drug formulation, indicating a reduced burst release of INH in the dual-drug system.[21] To elucidate the drug release mechanism from the drug-loaded NPs, the release data were fitted by using the Korsmeyer–Peppas model. In this study, the release exponent (n) for all NP formulations ranged between 0.43 and 0.85, indicating a non-Fickian diffusion process.[44] In other words, drug release was governed by a combination of polymer erosion and drug diffusion.

The reduced burst release of INH in dual-drug NPs was also reported by Yunus et al.,[21] who found that the presence of rifampicin in the NPs inhibited the release of levofloxacin. In this study, this effect was beneficial, as it reduced the initial burst release of INH and prolonged the subsequent sustained release phase. As a result, less INH was released prior to macrophage phagocytosis, allowing for higher drug concentrations within the macrophages. This slow and sustained release profile of the NPs is particularly advantageous for tuberculosis treatment, as it helps maintain therapeutic drug levels over an extended period, reduces the frequency of dosing, and minimizes dose-dependent toxicity and side effects.[45]

3.5. In Vitro Antibacterial Activity. The MICs of NPs and free drugs against MTB are presented in Figure 4. The

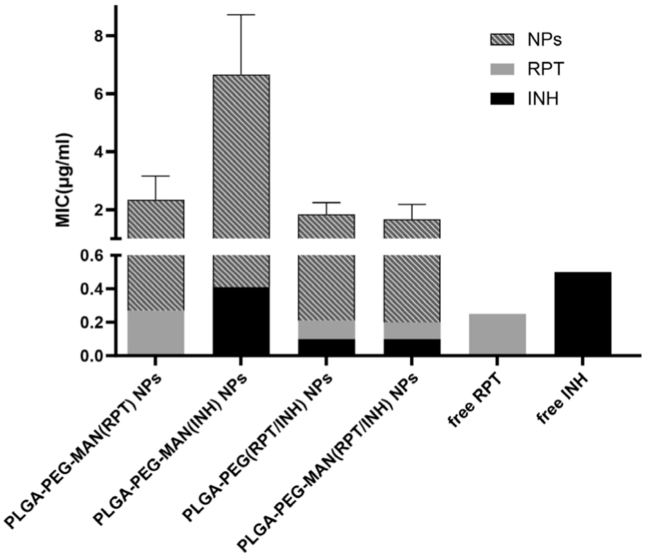

Figure 4. MIC of NPs and free drug.

MIC values for drug-loaded NPs, including PLGA–PEG-MAN (RPT) NPs, PLGA–PEG-MAN (INH) NPs, PLGA–PEG (RPT/INH) NPs, and PLGA–PEG-MAN (RPT/INH) NPs, were 2.33 ± 0.82, 6.67 ± 2.07, 1.83 ± 0.41, and 1.67 ± 0.52

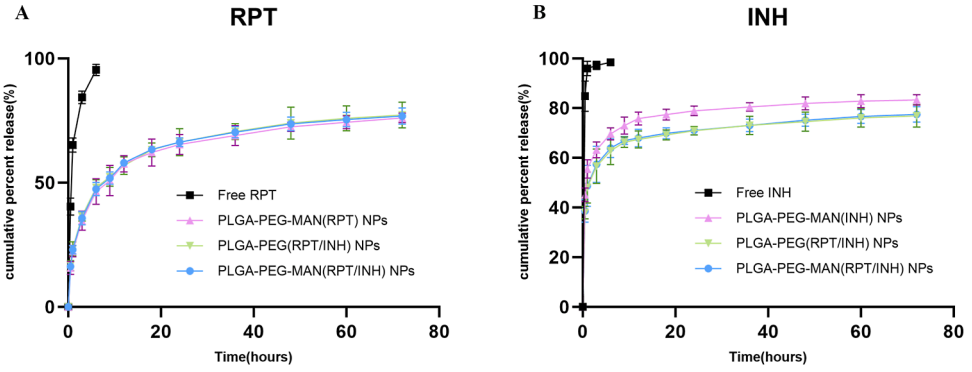

Figure 3. (A) In vitro RIF release from free RPT, PLGA–PEG-MAN (RPT) NPs, PLGA–PEG (RPT/INH) NPs, and PLGA–PEG-MAN (RPT/INH) NPs. (B) In vitro INH release from free INH, PLGA–PEG-MAN (INH) NPs, PLGA–PEG (RPT/INH) NPs, and PLGA–PEG-MAN (RPT/INH) NPs.

https://doi.org/10.1021/acs.bioconjchem.5c00062
Bioconjugate Chem. 2025, 36, 1021–1033

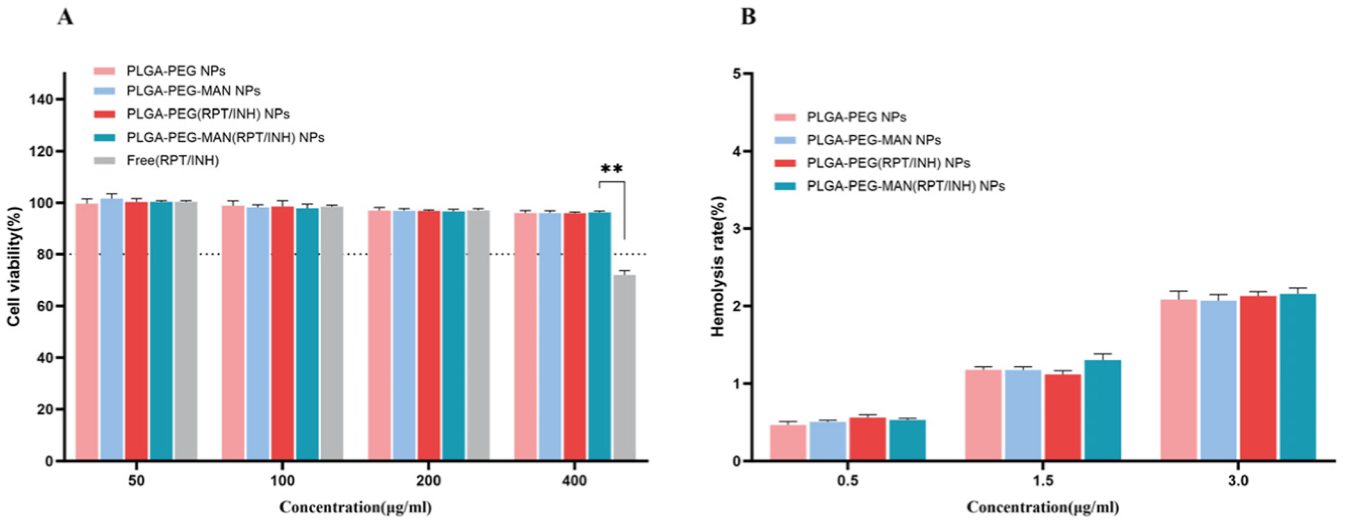

Figure 5. (A) Cytotoxicity studies of NPs on RAW 264.7 macrophage. (**$p < 0.01$) (B) hemolytic toxicity of various concentrations of NPs.

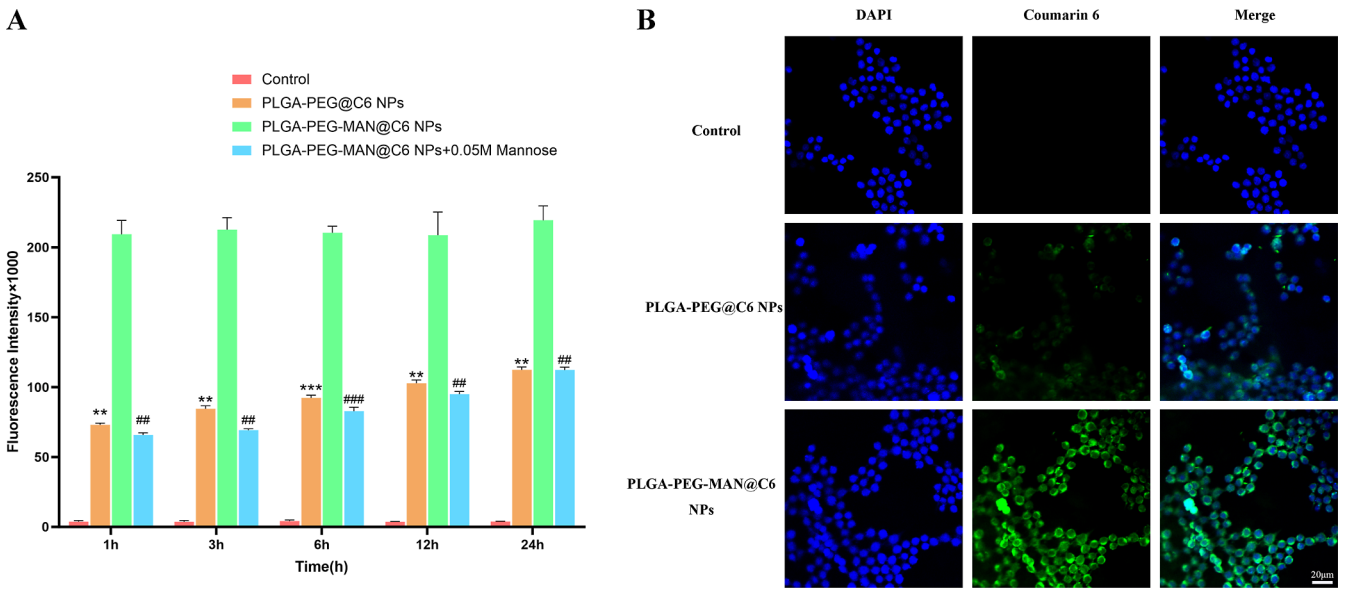

Figure 6. (A) Uptake of NPs by macrophages at different periods was expressed by fluorescence intensity measured by flow cytometry. Macrophages without NP treatment were used as the negative control. The PLGA−PEG-MAN@C6 NPs + 0.05 M Mannose group was a competitive receptor-blocking experiment performed to test whether MAN-modified NPs entered macrophages through mannose receptor-mediated phagocytosis. (**$p < 0.01$, ***$p < 0.001$, ##$p < 0.01$, ###$p < 0.001$ Compared to PLGA−PEG-MAN@C6 NP group.) (B) Fluorescent images showed cellular uptake of coumarin-6-labeled NPs by RAW 264.7 cells after 6 h coincubation. Coumarin 6 and DAPI were green and blue, respectively.

μg/mL, respectively. In comparison, the free drugs, RPT and INH, exhibited MIC values of 0.25 and 0.5 μg/mL, respectively. These MIC values for free drugs align with previously reported data, confirming the reliability of the MIC detection method used in this study.[18,46] The RPT contents in the four NP groups were 0.27, 0, 0.21, and 0.20 μg/mL, while the INH contents were 0, 0.41, 0.10, and 0.10 μg/mL, respectively, based on the calculated NP loading rates. The drug concentrations in the single-drug NPs were comparable to the MICs of the free drugs, indicating that the antibacterial activity of the drugs was retained during the loading process. For dual-drug NPs, the drug concentrations were below the MIC values of the free drugs, which may be attributed to the synergistic antibacterial activity of RPT and INH when delivered at the same time within the NPs.

Rifapentine, a long-acting rifamycin B antibiotic, targets the DNA-dependent RNA polymerase of MTB, inhibiting protein synthesis and suppressing bacterial growth and reproduction.[47] INH inhibits the synthesis of mycolic acid, a key component of the MTB cell wall, leading to loss of cell wall integrity, leakage of intracellular components, and ultimately bacterial growth inhibition or cell death.[48] Previous studies have demonstrated that combining rifamycin B antibiotics with INH significantly reduces MIC50 and MIC90 values compared to their individual use, highlighting their synergistic antibacterial effects.[49]

3.6. Cytotoxicity. The cytotoxicity of free drugs and the prepared NPs was evaluated by using the CCK-8 assay in RAW 264.7 macrophages (Figure 5A). Cell viability exceeded 95% at a concentration of 400 μg/mL for both drug-loaded and

https://doi.org/10.1021/acs.bioconjchem.5c00062
Bioconjugate Chem. 2025, 36, 1021−1033

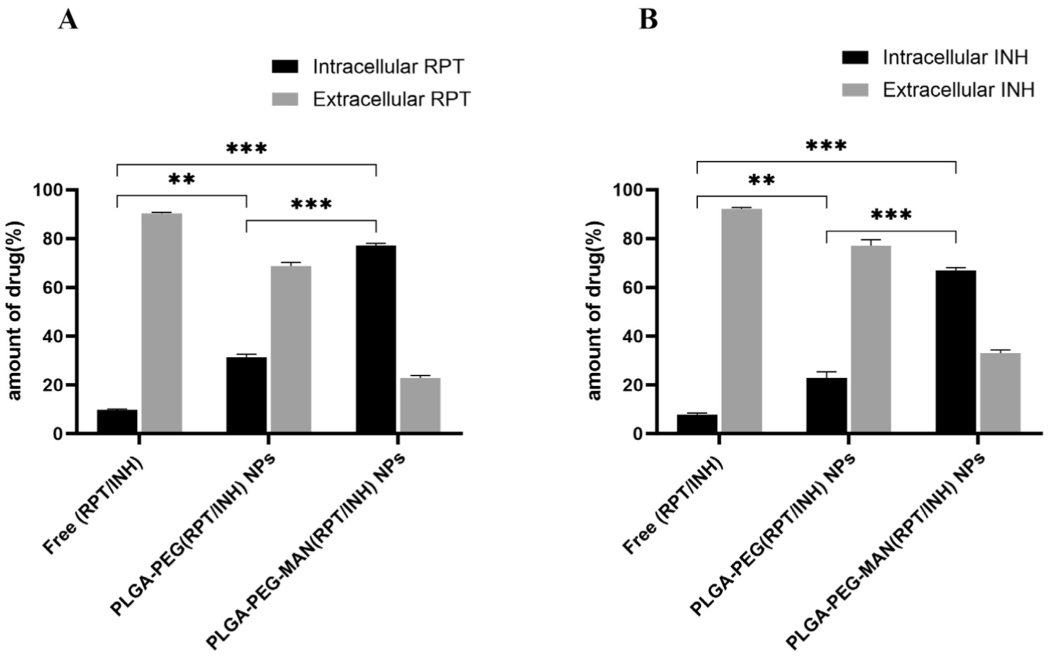

Figure 7. Intracellular and extracellular RPT (A) and INH (B) contents after coincubation of NPs or free drug with RAW 264.7 cells for 1 h. (**p < 0.01, ***p < 0.001).

nondrug-loaded NPs. In contrast, the free drug group exhibited only 72% cell viability at the equivalent drug concentration found in the PLGA−PEG-MAN (RPT/INH) NP group.

Cell viability above 80% is considered nontoxic according to the ISO 10993-5 standards.[50] These findings indicate that the prepared NPs were nontoxic and safe for RAW 264.7 cells at concentrations up to 400 μg/mL. In comparison, free drugs at equivalent concentrations demonstrated significant cytotoxicity. This indicates that encapsulating the drugs within NPs substantially reduces their cytotoxic effects while maintaining their therapeutic potential.

3.7. Hemolytic Toxicity. Regardless of the administration route—whether intravenous, oral, inhalation, or transdermal—NPs ultimately enter the bloodstream and interact with blood cells, particularly red blood cells, potentially causing hemolysis.[51] Nanomaterials are considered hemocompatible if the hemolysis rate remains below 5%, as per the criteria established by the American Society for Testing and Materials (ASTM).[52] The experimental results presented in Figure 5B demonstrate that the hemolysis rate increased with the NP concentration but remained well below the ASTM-defined threshold of 5%, even at concentrations significantly higher than those typically administered. Therefore, the NPs developed in this study are considered feasible for intravenous administration, enabling effective systemic drug delivery via the bloodstream.

3.8. Cell Uptake in Targeted Macrophages. To verify the macrophage-targeting ability of MAN-modified NPs, the uptake of fluorescently labeled NPs by RAW 264.7 macrophages was evaluated over 24 h by using flow cytometry and fluorescence microscopy. The results, presented in Figure 6A, indicate efficient internalization of both PLGA−PEG@C6 and PLGA−PEG-MAN@C6 NPs by macrophages, with PLGA−PEG-MAN@C6 NPs demonstrating significantly higher uptake at all time points. The enhanced uptake is attributed to mannose receptor-mediated phagocytosis. Figure 6B provides visual confirmation of these results, with macrophages treated with PLGA−PEG-MAN@C6 NPs exhibiting higher green fluorescence intensity compared to those treated with unmodified PLGA−PEG@C6 NPs after 6 h of coincubation. These findings highlight the enhanced macrophage-targeting capability of MAN-modified NPs, supporting their potential in targeted drug delivery for TB treatment. After 1 h of incubation, the fluorescence intensities detected in macrophages were 209×10^3 and 73×10^3 for PLGA−PEG-MAN@C6 NPs and PLGA−PEG@C6 NPs, respectively, indicating a 1.86-fold increase in macrophage internalization with MAN modification. The fluorescence intensity of PLGA−PEG-MAN@C6 NPs peaked at 1 h, with minimal increases observed thereafter. This observation is consistent with findings from Maretti et al.,[53] where mannosylated liposomes exhibited a fluorescence plateau within 15 min, indicating peak macrophage internalization. Similarly, Goyal et al.[54] reported peak internalization at 3 h, indicating that mannose receptor-mediated phagocytosis is a rapid process. At 24 h, MAN-modified NPs exhibited a 1.96-fold increase in macrophage internalization compared to unmodified NPs, despite the continued increase in internalization of the non-MAN-modified NPs.

To further assess the role of MAN modification in enhancing NP uptake by macrophages, a competitive inhibition experiment using free mannose was conducted. The results demonstrated that the uptake of PLGA−PEG-MAN@C6 NPs by RAW 264.7 macrophages was significantly reduced in the presence of free mannose (Figure 6A). These findings indicate that the enhanced uptake of PLGA−PEG-MAN@C6 NPs is primarily mediated by mannose receptor-mediated phagocytosis.

3.9. Drug Accumulation in RAW 264.7 Cells. The antibacterial efficacy of NPs against intracellular MTB depends significantly on the efficient delivery of encapsulated drugs into macrophages.[55] Figure 7 presents the intracellular and extracellular drug content in RAW 264.7 macrophages incubated with NPs or free drugs for 24 h. MAN-modified

https://doi.org/10.1021/acs.bioconjchem.5c00062
Bioconjugate Chem. 2025, 36, 1021−1033

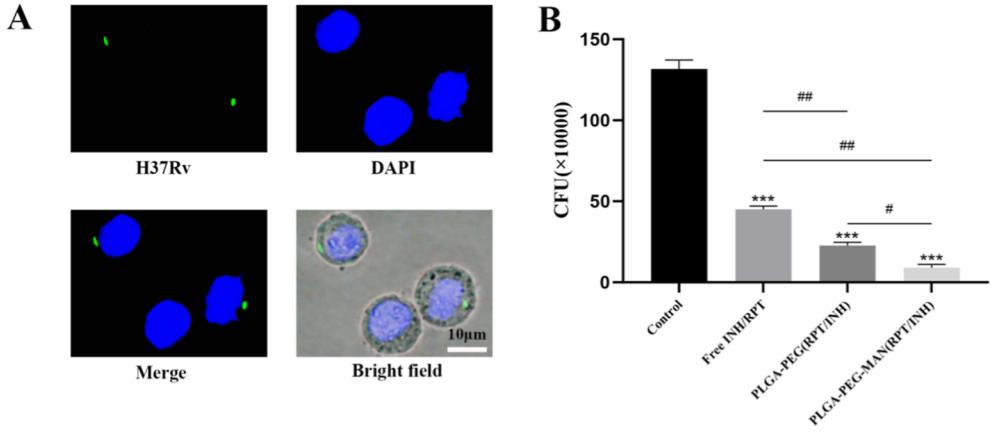

Figure 8. (A) Identification of H37Rv infection model in RAW 264.7 cells; (B) intracellular antibacterial activity of NPs. (***p < 0.001 vs control group; ##p < 0.01 vs free INH/RPT group; #p < 0.05 vs PLGA−PEG(RPT/INH) NP group).

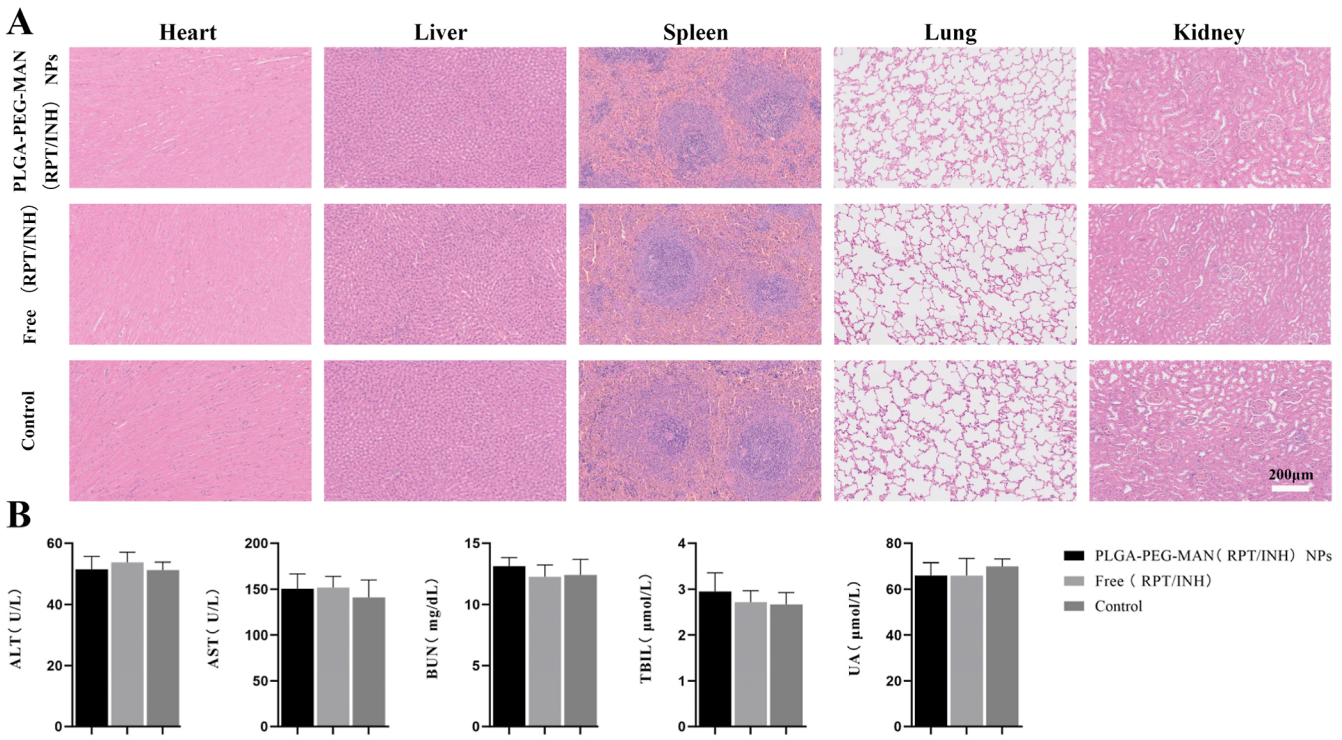

Figure 9. (A) H&E staining of the organs of rats and (A) serum biochemistry data.

drug-loaded NPs demonstrated significantly enhanced macrophage uptake with intracellular RPT levels 7.9-fold higher than the free drug and 2.5-fold higher than unmodified NPs. Similarly, INH levels were 8.5-fold higher than that of the free drug and 2.9-fold higher than that of unmodified NPs. These results highlight the substantial increase in the intracellular drug content achieved through MAN modification. The enhanced uptake of drugs into macrophages can be attributed to mannose receptor-mediated phagocytosis. MAN, by binding to the mannose receptor, facilitates the internalization of NPs by macrophages. Mannose-modified polymer NPs prepared by Patil et al.[56] delivered 72.46% of bedaquiline to macrophages within 12 h, which was significantly slower than the delivery rate observed in this study. Scanning electron microscopy revealed that the NPs had a PS exceeding 300 nm with a rough and irregular surface. Moreover, severe aggregation was observed, resulting in clusters with diameters larger than 20 μm. This aggregation likely hindered the rapid phagocytosis of NPs by macrophages.

Additionally, differences in the intracellular uptake of INH and RPT by RAW 264.7 cells were observed. Although both drugs were encapsulated within NPs and subsequently phagocytosed, in vitro release studies indicated that INH exhibited a significantly higher burst release rate during the initial phase compared to RPT. Consequently, a portion of INH was released into the extracellular culture medium before phagocytosis occurred, resulting in a relatively lower intracellular uptake of INH by RAW 264.7 cells when compared to RPT.

3.10. Intracellular Inhibition of *M. tuberculosis* by NPs. CLSM revealed green fluorescence surrounding the nuclei of RAW 264.7 cells, indicating the presence of H37Rv bacteria and confirming the successful establishment of the H37Rv infection model in RAW 264.7 cells (Figure 8A). The

https://doi.org/10.1021/acs.bioconjchem.5c00062
Bioconjugate Chem. 2025, 36, 1021−1033

results of the intracellular antibacterial activity of the NPs are shown in Figure 8B. Compared to those of the control group, both the free drugs and the dual drug-loaded NPs exhibited antibacterial effects. Notably, the drug-loaded NPs demonstrated superior intracellular antibacterial activity compared to the free drugs, and the mannosamine-modified NPs outperformed the unmodified ones. These findings from intracellular drug accumulation and antibacterial assays suggest that mannosamine modification significantly increased drug uptake by macrophages and effectively enhanced the antibacterial efficacy of the NPs within macrophages.

3.11. In Vivo Biosafety Study. H&E staining of the heart, liver, spleen, lungs, and kidneys revealed no apparent abnormalities (Figure 9A). Additionally, blood biochemical analysis showed no signs of hepatorenal toxicity in the drug-loaded NP group compared to the control group (Figure 9B, $P > 0.05$).

4. CONCLUSIONS

In this study, we successfully developed and synthesized MAN-modified RPT and INH-loaded PLGA−PEG NPs. The dual-drug-loaded NPs had an average PS of 117.67 nm and exhibited excellent physicochemical properties, with no observed cellular or hemolytic toxicity. The drug release profiles indicated a sustained release of both RPT and INH over 72 h, with no reduction in antimicrobial activity during the encapsulation process. The loaded drugs also demonstrated synergistic bactericidal effects. MAN modification significantly enhanced the phagocytosis of NPs by macrophages through mannose receptor-mediated internalization, thereby improving drug delivery efficiency and effectively boosting the antibacterial activity of the NPs within macrophages. In the in vivo study, pathological staining and biochemical analyses following intravenous injection revealed that the NPs did not produce any noticeable toxicity or adverse effects in rats. These findings indicate that MAN-modified RPT and INH-loaded PLGA−PEG NPs are promising candidates for macrophage-targeted anti-TB drug delivery.

AUTHOR INFORMATION

Corresponding Author

Xinghua Song − *Department of Spine Surgery, The Sixth Affiliated Hospital of Xinjiang Medical University, Urumqi, Xinjiang Uygur Autonomous Region 830002, China;* orcid.org/0000-0001-6208-4156; Phone: +86 13199836661; Email: songxinghua19@163.com

Authors

Cong Peng − *Department of Spine Surgery, The Sixth Affiliated Hospital of Xinjiang Medical University, Urumqi, Xinjiang Uygur Autonomous Region 830002, China*

Haopeng Luan − *Department of Spine Surgery, The Sixth Affiliated Hospital of Xinjiang Medical University, Urumqi, Xinjiang Uygur Autonomous Region 830002, China*

Qisong Shang − *Department of Spine Surgery, The Sixth Affiliated Hospital of Xinjiang Medical University, Urumqi, Xinjiang Uygur Autonomous Region 830002, China*

Wei Xiang − *Department of Spine Surgery, The Sixth Affiliated Hospital of Xinjiang Medical University, Urumqi, Xinjiang Uygur Autonomous Region 830002, China*

Parhat Yasin − *Department of Spine Surgery, The Sixth Affiliated Hospital of Xinjiang Medical University, Urumqi, Xinjiang Uygur Autonomous Region 830002, China*

Complete contact information is available at: https://pubs.acs.org/10.1021/acs.bioconjchem.5c00062

Author Contributions

†C.P. and H.L. authors contributed equally to this study. CP: conceptualization, data curation, formal analysis, software, writing—original draft, and writing—review and editing. HPL: conceptualization, data curation, formal analysis, software, and writing—review and editing. QSS: data curation, formal analysis, visualization. wx: data curation, and formal analysis. PY: software and writing—review and editing. XHS: conceptualization, funding acquisition, and writing—review and editing. All authors read and approved the final draft.

Notes

Ethics approval and consent to participate:This study was approved by the Animal Ethics Committee of the Animal Center of Xinjiang Medical University (approval no. IACUC-JT-20240711-18).

The authors declare no competing financial interest.

ACKNOWLEDGMENTS

The study was funded by the National Natural Science Foundation of China (82172454).

REFERENCES

(1) Shabil, M.; Bushi, G.; Beig, M. A.; et al. Cardiovascular Manifestation in Tuberculosis Cases: A Systematic Review and Meta-Analysis. *Curr. Probl. Cardiol.* **2023**, *48* (7), 101666.

(2) World Health Organization. Global tuberculosis report 2024, 2024. https://www.who.int/publications/i/item/9789240101531.

(3) van der Wel, N.; Hava, D.; Houben, D.; et al. M. tuberculosis and M. leprae translocate from the phagolysosome to the cytosol in myeloid cells. *Cell* **2007**, *129* (7), 1287−1298.

(4) Gehring, A. J.; Dobos, K. M.; Belisle, J. T.; Harding, C. V.; Boom, W. H. Mycobacterium tuberculosis LprG (Rv1411c): a novel TLR-2 ligand that inhibits human macrophage class II MHC antigen processing. *J. Immunol.* **2004**, *173* (4), 2660−2668.

(5) Zhai, W.; Wu, F.; Zhang, Y.; Fu, Y.; Liu, Z. The Immune Escape Mechanisms of Mycobacterium Tuberculosis. *Int. J. Mol. Sci.* **2019**, *20* (2), 340.

(6) Dartois, V. The path of anti-tuberculosis drugs: from blood to lesions to mycobacterial cells. *Nat. Rev. Microbiol.* **2014**, *12* (3), 159−167.

(7) Weeratunga, P.; Moller, D. R.; Ho, L. P. Immune mechanisms of granuloma formation in sarcoidosis and tuberculosis. *J. Clin. Invest.* **2024**, *134* (1), No. e175264.

(8) Wang, H.; Li, B.; Sun, Y.; Ma, Q.; Feng, Y.; Jia, Y.; Wang, W.; Su, M.; Liu, X.; Shu, B.; et al. NIR-II AIE Luminogen-Based Erythrocyte-Like Nanoparticles with Granuloma-Targeting and Self-Oxygenation Characteristics for Combined Phototherapy of Tuberculosis. *Adv. Mater.* **2024**, *36* (38), No. e2406143.

(9) Laws, M.; Jin, P.; Rahman, K. M. Efflux pumps in Mycobacterium tuberculosis and their inhibition to tackle antimicrobial resistance. *Trends Microbiol.* **2022**, *30* (1), 57−68.

(10) Gairola, A.; Benjamin, A.; Weatherston, J. D.; Cirillo, J. D.; Wu, H. J. Recent Developments in Drug Delivery for Treatment of Tuberculosis by Targeting Macrophages. *Adv. Ther.* **2022**, *5* (6), 2100193.

(11) Cummings, R. D. The mannose receptor ligands and the macrophage glycome. *Curr. Opin. Struct. Biol.* **2022**, *75*, 102394.

(12) Embgenbroich, M.; van der Zande, H.; Hussaarts, L.; Schulte-Schrepping, J.; Pelgrom, L. R.; García-Tardón, N.; Schlautmann, L.; Stoetzel, I.; Händler, K.; Lambooij, J. M.; et al. Soluble mannose receptor induces proinflammatory macrophage activation and metaflammation. *Proc. Natl. Acad. Sci. U.S.A.* **2021**, *118* (31), No. e2103304118.

(13) Yusuf, A.; Almotairy, A.; Henidi, H.; Alshehri, O. Y.; Aldughaim, M. S. Nanoparticles as Drug Delivery Systems: A Review of the Implication of Nanoparticles' Physicochemical Properties on Responses in Biological Systems. *Polymers* **2023**, *15* (7), 1596.
(14) Zielińska, A.; Carreiro, F.; Oliveira, A. M.; Neves, A.; Pires, B.; Venkatesh, D. N.; Durazzo, A.; Lucarini, M.; Eder, P.; Silva, A. M.; et al. Polymeric Nanoparticles: Production, Characterization, Toxicology and Ecotoxicology. *Molecules* **2020**, *25* (16), 3731.
(15) Mir, M.; Ahmed, N.; Rehman, A. U. Recent applications of PLGA based nanostructures in drug delivery. *Colloids Surf., B* **2017**, *159*, 217−231.
(16) Xu, Q.; Ensign, L. M.; Boylan, N. J.; et al. Impact of Surface Polyethylene Glycol (PEG) Density on Biodegradable Nanoparticle Transport in Mucus ex Vivo and Distribution in Vivo. *ACS Nano* **2015**, *9* (9), 9217−9227.
(17) Zhang, K.; Tang, X.; Zhang, J.; et al. PEG-PLGA copolymers: their structure and structure-influenced drug delivery applications. *J. Controlled Release* **2014**, *183*, 77−86.
(18) Liang, Q.; Xiang, H.; Li, X.; et al. Development of Rifapentine-Loaded PLGA-Based Nanoparticles: In vitro Characterisation and in vivo Study in Mice. *Int. J. Nanomed.* **2020**, *15*, 7491−7507.
(19) Pi, J.; Chen, D.; Wang, J.; et al. Macrophage targeted graphene oxide nanosystem synergize antibiotic killing and host immune defense for Tuberculosis Therapy. *Pharmacol. Res.* **2024**, *208*, 107379.
(20) Sumaila, M.; Kumar, P.; Ubanako, P.; Adeyemi, S. A.; Choonara, Y. E. Dual Rifampicin and Isoniazid Mannose-Decorated Lipopolysaccharide Nanospheres for Macrophage- Targeted Lung Delivery. *Curr. Drug Delivery* **2023**, *20* (10), 1487−1503.
(21) Yunus, B. R.; T, S. S.; Doble, M. Dual delivery of tuberculosis drugs via cyclodextrin conjugated Curdlan nanoparticles to infected macrophages. *Carbohydr. Polym.* **2019**, *218*, 53−62.
(22) Puri, V.; Chaudhary, K. R.; Singh, A.; Singh, C. Inhalation potential of N-Acetylcysteine loaded PLGA nanoparticles for the management of tuberculosis: In vitro lung deposition and efficacy studies. *Curr. Res. Pharmacol. Drug Discov.* **2022**, *3*, 100084.
(23) Toro-Gonzalez, M.; Akingbesote, N.; Bible, A.; Pal, D.; Sanders, B.; Ivanov, A. S.; Jansone-Popova, S.; Popovs, I.; Benny, P.; Perry, R.; et al. Development of (225)Ac-doped biocompatible nanoparticles for targeted alpha therapy. *J. Nanobiotechnol.* **2024**, *22* (1), 306.
(24) Intorasoot, S.; Intorasoot, A.; Tawteamwong, A.; Butr-Indr, B.; Phunpae, P.; Tharinjaroen, C. S.; Wattananandkul, U.; Sangboonruang, S.; Khantipongse, J. In Vitro Antimycobacterial Activity of Human Lactoferrin-Derived Peptide, D-hLF 1−11, against Susceptible and Drug-Resistant Mycobacterium tuberculosis and Its Synergistic Effect with Rifampicin. *Antibiotics* **2022**, *11* (12), 1785.
(25) Liang, Q.; Zhang, P.; Zhang, L.; Luan, H.; Li, X.; Xiang, H.; Jing, S.; Song, X. Development of tetracycline-modified nanoparticles for bone-targeted delivery of anti-tubercular drug. *Front. Bioeng. Biotechnol.* **2023**, *11*, 1207520.
(26) Tiwari, S.; Chaturvedi, A. P.; Tripathi, Y. B.; Mishra, B. Macrophage-specific targeting of isoniazid through mannosylated gelatin microspheres. *AAPS PharmSciTech* **2011**, *12* (3), 900−908.
(27) Danaei, M.; Dehghankhold, M.; Ataei, S.; Hasanzadeh Davarani, F.; Javanmard, R.; Dokhani, A.; Khorasani, S.; Mozafari, M. R. Impact of Particle Size and Polydispersity Index on the Clinical Applications of Lipidic Nanocarrier Systems. *Pharmaceutics* **2018**, *10* (2), 57.
(28) Kulkarni, S. A.; Feng, S. S. Effects of particle size and surface modification on cellular uptake and biodistribution of polymeric nanoparticles for drug delivery. *Pharm. Res.* **2013**, *30* (10), 2512−2522.
(29) de Barros, A. B.; Tsourkas, A.; Saboury, B.; Cardoso, V. N.; Alavi, A. Emerging role of radiolabeled nanoparticles as an effective diagnostic technique. *EJNMMI Res.* **2012**, *2* (1), 39.
(30) Moghimi, S. M.; Hunter, A. C.; Andresen, T. L. Factors controlling nanoparticle pharmacokinetics: an integrated analysis and perspective. *Annu. Rev. Pharmacol. Toxicol.* **2012**, *52*, 481−503.
(31) Chan, H. W.; Chow, S.; Zhang, X.; Kwok, P.; Chow, S. F. Role of Particle Size in Translational Research of Nanomedicines for Successful Drug Delivery: Discrepancies and Inadequacies. *J. Pharm. Sci.* **2023**, *112* (9), 2371−2384.
(32) Ozturk, K.; Kaplan, M.; Calis, S. Effects of nanoparticle size, shape, and zeta potential on drug delivery. *Int. J. Pharm.* **2024**, *666*, 124799.
(33) Carneiro, S. P.; Carvalho, K. V.; de Oliveira, A. S. R.; et al. Functionalized rifampicin-loaded nanostructured lipid carriers enhance macrophages uptake and antimycobacterial activity. *Colloids Surf., B* **2019**, *175*, 306−313.
(34) Zhu, J.; Qin, F.; Ji, Z.; Fei, W.; Tan, Z.; Hu, Y.; Zheng, C. Mannose-Modified PLGA Nanoparticles for Sustained and Targeted Delivery in Hepatitis B Virus Immunoprophylaxis. *AAPS PharmSciTech* **2019**, *21* (1), 13.
(35) Bashir, S.; Shabbir, K.; Din, F. U.; et al. Nitazoxanide and quercetin co-loaded nanotransfersomal gel for topical treatment of cutaneous leishmaniasis with macrophage targeting and enhanced anti-leishmanial effect. *Heliyon* **2023**, *9* (11), No. e21939.
(36) Yoo, J. W.; Chambers, E.; Mitragotri, S. Factors that control the circulation time of nanoparticles in blood: challenges, solutions and future prospects. *Curr. Pharm. Des.* **2010**, *16* (21), 2298−2307.
(37) Haggag, Y.; Abdel-Wahab, Y.; Ojo, O.; et al. Preparation and in vivo evaluation of insulin-loaded biodegradable nanoparticles prepared from diblock copolymers of PLGA and PEG. *Int. J. Pharm.* **2016**, *499* (1−2), 236−246.
(38) Samuelsson, E.; Shen, H.; Blanco, E.; Ferrari, M.; Wolfram, J. Contribution of Kupffer cells to liposome accumulation in the liver. *Colloids Surf., B* **2017**, *158*, 356−362.
(39) Patil, S.; Sandberg, A.; Heckert, E.; Self, W.; Seal, S. Protein adsorption and cellular uptake of cerium oxide nanoparticles as a function of zeta potential. *Biomaterials* **2007**, *28* (31), 4600−4607.
(40) Ma, C.; Wu, M.; Ye, W.; et al. Inhalable solid lipid nanoparticles for intracellular tuberculosis infection therapy: macrophage-targeting and pH-sensitive properties. *Drug Delivery Transl. Res.* **2021**, *11* (3), 1218−1235.
(41) Upadhyay, T. K.; Fatima, N.; Sharma, A.; Sharma, D.; Sharma, R. Nano-Rifabutin entrapment within glucan microparticles enhances protection against intracellular Mycobacterium tuberculosis. *Artif. Cells, Nanomed., Biotechnol.* **2019**, *47* (1), 427−435.
(42) Shrivastava, P.; Gautam, L.; Sharma, R.; et al. Dual antitubercular drug loaded liposomes for macrophage targeting: development, characterisation, ex vivo and in vivo assessment. *J. Microencapsulation* **2021**, *38* (2), 108−123.
(43) Hoshyar, N.; Gray, S.; Han, H.; Bao, G. The effect of nanoparticle size on in vivo pharmacokinetics and cellular interaction. *Nanomedicine* **2016**, *11* (6), 673−692.
(44) Wei, W.; Li, S.; Xu, H.; et al. MPEG-PCL Copolymeric Micelles for Encapsulation of Azithromycin. *AAPS PharmSciTech* **2018**, *19* (5), 2041−2047.
(45) Prabhu, P.; Fernandes, T.; Chaubey, P.; et al. Mannose-conjugated chitosan nanoparticles for delivery of Rifampicin to Osteoarticular tuberculosis. *Drug Delivery Transl. Res.* **2021**, *11* (4), 1509−1519.
(46) Heinrichs, M. T.; May, R. J.; Heider, F.; et al. Mycobacterium tuberculosis Strains H37ra and H37rv have equivalent minimum inhibitory concentrations to most antituberculosis drugs. *Int. J. Mycobact.* **2018**, *7* (2), 156−161.
(47) Yoshikawa, T. T.; Fujita, N. K. Antituberculous drugs. *Med. Clin. North Am.* **1982**, *66* (1), 209−219.
(48) Rastogi, N.; David, H. L. Mode of action of antituberculous drugs and mechanisms of drug resistance in Mycobacterium tuberculosis. *Res. Microbiol.* **1993**, *144* (2), 133−143.
(49) Ying, R.; Huang, X.; Gao, Y.; et al. In vitro Synergism of Six Antituberculosis Agents Against Drug-Resistant Mycobacterium tuberculosis Isolated from Retreatment Tuberculosis Patients. *Infect. Drug Resist.* **2021**, *14*, 3729−3736.
(50) Lopez-Garcia, J.; Lehocky, M.; Humpolicek, P.; Saha, P. HaCaT Keratinocytes Response on Antimicrobial Atelocollagen

Substrates: Extent of Cytotoxicity, Cell Viability and Proliferation. *J. Funct. Biomater.* **2014**, *5* (2), 43−57.
(51) Yedgar, S.; Barshtein, G.; Gural, A. Hemolytic Activity of Nanoparticles as a Marker of Their Hemocompatibility. *Micromachines* **2022**, *13* (12), 2091.
(52) Xiao, Y.; Zhang, M.; Fan, Y.; et al. Novel controlled drug release system engineered with inclusion complexes based on carboxylic graphene. *Colloids Surf., B* **2019**, *175*, 18−25.
(53) Maretti, E.; Costantino, L.; Rustichelli, C.; et al. Surface engineering of Solid Lipid Nanoparticle assemblies by methyl alpha-d-mannopyranoside for the active targeting to macrophages in anti-tuberculosis inhalation therapy. *Int. J. Pharm.* **2017**, *528* (1−2), 440−451.
(54) Goyal, A. K.; Garg, T.; Rath, G.; Gupta, U. D.; Gupta, P. Development and Characterization of Nanoembedded Microparticles for Pulmonary Delivery of Antitubercular Drugs against Experimental Tuberculosis. *Mol. Pharmaceutics* **2015**, *12* (11), 3839−3850.
(55) Maretti, E.; Costantino, L.; Buttini, F.; et al. Newly synthesized surfactants for surface mannosylation of respirable SLN assemblies to target macrophages in tuberculosis therapy. *Drug Delivery Transl. Res.* **2019**, *9* (1), 298−310.
(56) Patil, S. M.; Daram, A.; Kunda, N. K. 3D spheroid model reveals enhanced efficacy of mannose-decorated nanoparticles for TB treatment. *Nanomedicine* **2025**, *20*, 777−789.

https://doi.org/10.1021/acs.bioconjchem.5c00062
Bioconjugate Chem. 2025, 36, 1021−1033